Carbohydrate Polymers 329 (2024) 121757

Contents lists available at ScienceDirect

Carbohydrate Polymers

journal homepage: www.elsevier.com/locate/carbpol

Does harvesting age matter? Changes in structure and rheology of a shear-thickening polysaccharide from *Cyathea medullaris* as a function of age

Akshay Bisht [a], Kelvin K.T. Goh [a], Ian M. Sims [b], Patrick J.B. Edwards [c], Lara Matia-Merino [a,*]

[a] School of Food and Advanced Technology, Massey University, Palmerston North, New Zealand
[b] The Ferrier Research Institute, Victoria University of Wellington, New Zealand
[c] School of Natural Sciences, Massey University, Palmerston North, New Zealand

ARTICLE INFO

Keywords:
Mamaku polysaccharide
Shear-thickening
Molecular structure
Shear rheology
Extensional rheology

ABSTRACT

A shear-thickening polysaccharide from the New Zealand Black tree fern (*Cyathea medullaris*, commonly known as mamaku) extracted from different age fronds (stage 1: young, stage 2: fully grown and stage 3: old) was characterised in terms of structure and rheological properties. Constituent sugar analysis and ^{1}H and ^{13}C NMR revealed a repeating backbone of −4)-β-D-Glc*p*A-(1 → 2)-α-D-Man*p*-(1→, for all mamaku polysaccharide (MP) samples from different age fronds without any alterations in molecular structure. However, the molecular weight (M_w) was reduced with increasing age, from ~4.1 × 10^6 to ~2.1 × 10^6 Da from stage 1 to stage 3, respectively. This decrease in M_w (and size) consequently reduced the shear viscosity ($\eta_{s\text{-}Stage\ 1} > \eta_{s\text{-}Stage\ 2} > \eta_{s\text{-}Stage\ 3}$). However, the extent of shear-thickening and uniaxial extensional viscosity of MP stage 2 was greater than MP stage 1, which was attributed to a greater intermolecular interaction occurring in the former. Shear-thickening behaviour was not observed in MP stage 3.

1. Introduction

Consumer demand for minimally processed natural ingredients is recognised by the scientific community, and therefore attempts are constantly being made to seek novel ingredients, such as polysaccharides, to be used in the pharmaceutical, nutraceutical, cosmetic and food industries. Here we study a novel water-soluble polysaccharide from the New Zealand black tree fern (*Cyathea medullaris*), commonly known as mamaku.

The reddish-brown mucilage from mamaku pith was first characterised for its rheological behaviour by our group in 2007 (Goh, Matia-Merino, Hall, Moughan, & Singh, 2007). It was reported that mamaku mucilage exhibits unique rheological properties such as Newtonian, shear-thickening, shear-thinning, thixotropic and anti-thixotropic behaviour (depending on concentration and shear rate). Shear-thickening behaviour is generally reported for synthetic polymers (Chen et al., 2019; Hu, Wang, & Jamieson, 1995; Ma & Cooper, 2001; Tam, Jenkins, Winnik, & Bassett, 1998; Tan, Tam, & Jenkins, 2001; Xu, Hawk, Loveless, Jeon, & Craig, 2010) and for physically/chemically modified natural polymers (Ang, Goh, Lim, & Matia-Merino, 2021; Burckbuchler et al., 2006; Kjøniksen, Hiorth, & Nyström, 2005); however, is not a common phenomenon in unmodified natural polymers. The complex rheological behaviour of mamaku mucilage was attributed to the presence of a non-starch polysaccharide fraction referred to as mamaku polysaccharide (MP). MP is a long-chain glucuronomannan polymer comprising of a repeating backbone of β-1,4-linked methyl-esterified glucopyranosyl uronic acid and α-1,2-linked mannopyranosyl residues, branched at O-3 of 45 % and at both O-3 and O-4 of 53 % of the mannopyranosyl residues (Wee, Matia-Merino, Carnachan, Sims, & Goh, 2014). The sidechain consists of galactose, arabinose, non-methylesterified glucuronic acid and other simple sugars. Furthermore, MP was reported to have strong extensional viscosity (η_e—of the order 10^3) (Jaishankar, Wee, Matia-Merino, Goh, & McKinley, 2015) indicating higher intermolecular interaction between MP chains during extension as compared to other polymers such as guar gum (Szopinski, Handge, Kulicke, Abetz, & Luinstra, 2016) or okra polysaccharide (Yuan, Ritzoulis, & Chen, 2018).

Studies disclosing novel polysaccharides from natural sources are

* Corresponding author.
E-mail addresses: A.Bisht@massey.ac.nz (A. Bisht), K.T.Goh@massey.ac.nz (K.K.T. Goh), Ian.Sims@vuw.ac.nz (I.M. Sims), P.J.Edwards@massey.ac.nz (P.J.B. Edwards), L.Matia-Merino@massey.ac.nz (L. Matia-Merino).

https://doi.org/10.1016/j.carbpol.2023.121757
Received 15 October 2023; Received in revised form 21 December 2023; Accepted 28 December 2023
Available online 3 January 2024

common in the literature, although, the relatively small amount of information available limits their use for commercial applications. It is vital to understand the properties of novel polysaccharides at all stages of their development, *i.e.*, from their origin to end-use. During biochemical and physiological developments in the plant, such as seed germination and fruit ripening, endogenous enzymes can cause structural changes in polysaccharides (Ward, Moo-Young, & Venkat, 1989), thereby affecting their functionality. During the ripening of fruits, the activity of several enzymes such as pectin esterases, responsible for the changes in pectin structure, increases significantly (Wang, Yeats, Uluisik, Rose, & Seymour, 2018). Changes in pectin during maturation may include shortening of the pectin chain, demethylation of carboxyl groups and deacetylation of hydroxyl groups (Ward et al., 1989). Therefore, it is important to understand the effect of mamaku frond age on the functionality of MP.

Our working hypothesis is that the physicochemical properties of MP differ as a function of age, which affects its functionality (*e.g.*, shear and extensional rheology). This work not only provides useful knowledge on the appropriate and sustainable harvesting time but also on how to achieve product uniformity in large-scale production. To the best of our knowledge, there is no report characterising the changes in MP based on the age of fronds. In this study, we present a comprehensive analysis of the structural characterisation of MP extracted from three different age group fronds and its impact on shear and uniaxial extensional rheology.

2. Material and methods

2.1. Extraction and purification of mamaku gum

Mamaku fronds from three different age groups were harvested from seven different ferns from a farm at Waverley, Taranaki, New Zealand, between the 10th and 30th of October 2020 following local practices. The harvesting stages were classified based on the significant visual changes in the growth of the fern. Stage 1 refers to young fronds (also known as *koru*), stage 2 refers to fully grown fronds, while stage 3 refers to fronds starting to die, where brown sections were observed (Fig. A1). Gum extraction was carried out as described by Bisht, Goh, and Matia-Merino (2023), with some modifications. Briefly, the fronds were chopped, blended with water and heated to ~55 °C for 5 min with continuous stirring. The exuded gum, separated from insoluble plant debris, was collected. The left-over pulp was reheated in water and the extract was collected until no visual viscous consistency of the flowing liquid was observed. This was repeated an average of 3–5 cycles. The pooled extracts were left undisturbed overnight at 4 °C for the remains of pulp to sediment by gravity. The clearer top layer was then separated using a siphon, and the 'crude gum' freeze-dried.

The crude mamaku gum extract samples were hydrated overnight (5 % w/w) and ultra-centrifuged (Sorvall WX Ultra 100, T-865 motor, Thermo-Fisher Scientific, Waltham, Massachusetts, USA) at 250,000*g* for 1 h to remove large aggregates, dialysed (molecular weight cut-off: 12,000–14,000 Da) against reducing NaCl concentrations (0.01 M, 0.001 M and milli-Q water only) for ~42 h at 4 °C, and the 'purified gum fraction' freeze-dried.

2.2. Chemical analysis

Quantification of total solids, ash, protein, fat, starch and dietary fibres (soluble and insoluble) was carried out on the crude gum extracts using AOAC 925.45A, AOAC 942.05, AOAC 968.06, AOAC 922.06, AOAC 996.11 (Megazyme kit) and AOAC 991.43 (Megazyme kit) methods, respectively. The mineral and sugar compositions were analysed using an inductively coupled plasma (ICP)-optical emission spectrometer and gas chromatography, respectively. The uronic acid content was quantified spectrophotometrically using the *m*-hydroxydiphenyl method with glucuronic acid as the standard (Blumenkrantz & Asboe-Hansen, 1973). The chemical analyses were conducted by an accredited Nutrition Laboratory, Massey University, Palmerston North, New Zealand.

2.3. Constituent sugar analysis

The constituent sugar composition of purified gum was determined using high-performance anion-exchange chromatography (HPAEC) after hydrolysis to its component monosaccharides, as described by De Ruiter, Schols, Voragen, and Rombouts (1992) with modifications (Wee et al., 2014). Briefly, duplicate samples (400 μg) were hydrolysed with methanolic HCl (3 M, 500 μl, 80 °C, 18 h), followed by aqueous trifluoroacetic acid (TFA, 2.5 M, 500 μl, 120 °C, 1 h). The resulting hydrolysates were dried, diluted with Type 1 water (to 80 μg/ml) and analysed on a CarboPac PA-1 (4 × 250 mm) column equilibrated in 20 mM NaOH and eluted with a simultaneous gradient of NaOH and NaOAc at 30 °C and a flow rate of 1 ml/min. The sugars were identified from their elution times relative to a standard sugar mix (L-fucose, L-rhamnose, L-arabinose, D-galactose, D-glucose, D-mannose, D-xylose, D-galacturonic acid, and D-glucuronic acid), and quantified from the response calibration curves of each sugar.

2.4. NMR

The purified mamaku gum samples were deuterium exchanged by freeze-drying twice with D_2O and dissolved in D_2O at 6.7 mg/ml, with the addition of acetone (0.4 % v/v) as an internal standard, set at 31.45 ppm (^{13}C) and 2.225 ppm (^{1}H). NMR data were collected on a Bruker Avance Neo 700 MHz NMR spectrometer (Bruker BioSpin, Rheinstetten, Germany), equipped with a 5 mm TCI cryoprobe (fitted with a Z-gradient coil), at 65 °C. 1D ^{1}H NMR spectra were recorded with a spectral width of 20 ppm, 65,536 complex data points, 30-degree excitation pulse, each with an acquisition time of 2.36 s and a 1 s recycle delay time. Phase-sensitive, sensitivity enhanced Heteronuclear single quantum coherence (HSQC) and double-quantum filtered correlation spectroscopy (DQF-COSY) experiments were carried out using standard Bruker pulse programs (*hsqcetgpsisp2.2* and *cosydfph*). The 2D spectra used spectral widths of 10.2 and 124.0 ppm for the ^{1}H and ^{13}C dimensions, respectively. The HSQC was digitized using 2048 × 320 points. The DQF-COSY was acquired using 50 % non-uniform sampling in the indirect dimension, giving a final data matrix of 2048 × 400 points. Both 2D experiments used a recycle delay of 1.5 s. Spectra were analysed and processed in Mestranova (Version 14.1.2). Assignments were made by comparing the spectra with published data.

2.5. Size-exclusion chromatography coupled with multi-angle laser light scattering (SEC-MALLS)

The weight-average molar mass (M_w) and root mean square radius (R_z) for purified gum samples was determined using high-performance liquid chromatography (HPLC) system (Shimadzu, Kyoto, Japan) coupled with multi-angle laser light scattering (Dawn Heleos 8+, Wyatt Technology Corp., Goleta, California, USA), as described by Bisht, Goh, Sims, Edwards, and Matia-Merino (2023). Separation was achieved by connecting two size-exclusion columns in series with a guard column (OHpak SB-G, SB-804 HQ and SB-806 M HQ columns, Shodex, Tokyo, Japan) at 25 °C. The purified gum samples were centrifuged at 30,000*g* for 1 h, followed by injection (20 μl) into the HPLC system at a flow rate of 0.5 ml/min and eluted with 0.1 M NaCl. The Astra software (Version 6.1.1.17, Wyatt Technology) was used to analyse the light scattering peak using the Zimm plot at an incremental refractive index (*dn/dc*) of 0.178 ml/g.

2.6. Shear rheology

Freeze-dried crude gum extract was hydrated in milli-Q water at different total solid concentrations (w/w) for ~15 h at 20 °C.

Rheological measurements were performed using a Paar Physica MCR 302 rheometer (Anton-Paar, Graz, Austria) in controlled shear rate (CSR) mode using a log-ramp profile from 30 s to 2 s (initial to final) at 20.0 ± 0.1 °C. Viscosity profiles were measured using the cup-and-bob geometry (CC27 and C-PTD 200) and data were recorded using Rheoplus/32 software (Version 3.62).

Oscillatory measurements (frequency sweep) were performed in the range of 0.01–20 Hz using a constant strain value of 5 % (within the linear viscoelastic region) using the double gap geometry (DG-26-7 and C-PTD 200). The samples after loading were allowed to rest for 5 min, before starting the experiment, to reduce any effect of shear-history and for temperature equilibration.

2.7. Extensional rheology

The extensional behaviour of crude gum extract was investigated using a portable capillary-breakup extensional rheometer, built in-house at Massey University based on the design described by Hallmark et al. (2016). This instrument consists of two cylindrical pistons of diameter, D_o, 4 mm separated by an initial gap, L_o, 1.5 mm (giving initial aspect ratio, $\Lambda_o = L_o/D_o = 0.38$). The samples were loaded between the pistons (cylindrical volume of fluid ~0.02 ml) and the top piston was displaced instantaneously to the final separation, L_f, of 4 mm (giving final aspect ratio, $\Lambda_f = L_f/D_o = 1$) using a battery-powered solenoid to impose a predominantly uniaxial extensional deformation and thus, create a liquid filament bridge between pistons. The subsequent evolution of the liquid filament diameter was monitored using a high-speed camera at 500 frames per second. MATLAB software was programmed to digitally analyse the measurements of the diameter in each frame. The experiment was repeated at least 10 times in a temperature-controlled room at 20 °C.

The filament thinning experiment assumes axial symmetry about the midplane but is strongly influenced by gravitational force, causing filament sagging. In order to minimize gravitational sagging and obtain the initial filament configuration close to the cylinder, the experiment parameters were set such that $L_o \leq$ capillary length, $l_{cap} = \sqrt{\sigma}/\rho g \approx 2.5$ mm, or equivalently $2L_o/D_o \leq 1/\sqrt{B_o} \approx 0.75 \leq 1.3$; where σ is surface tension, ρ is density (assumed as 1000 kg/m^3), g is the acceleration due to gravity (9.18 m/s^2) and B_o is Bond number ($= \frac{\rho g D_o^2}{4\sigma} \approx 0.6$) (Rodd, Scott, Cooper-White, & McKinley, 2005). The surface tension for all the samples was measured independently using a Tensiometer (Biolin Scientific Attention theta flex, ATA Scientific Instruments, Australia) (Table A1).

The liquid filament thins under the action of viscous, elastic and capillary forces and the midplane diameter, $D(t)$, of the filament varies as a function of time. Three characteristic diameters were recorded for analysis: D_o, the initial sample diameter (≈ piston diameter = 4 mm); D_1, the diameter of mid-filament immediately after stretching; and $D(t)$, is the change in filament diameter with time after stretching until breakup. For viscous Newtonian fluids of viscosity η_s and surface tension σ, the midplane diameter, $D(t)$, decays linearly with time until breakup according to

$$D(t) = 0.0709\frac{2\sigma}{\eta_s}(tb - t) \quad (1)$$

where t_b is the capillary breakup time (McKinley & Tripathi, 2000). However, for viscoelastic fluids, the filament initially drains under capillary pressure which is restricted predominantly by viscosity stress. The extensional flow generated during thinning results in additional elastic stress, due to the deformation of microstructure, which grows with increasing strain and ultimately dominates the viscous stress. This point, when capillary pressure arising from surface tension is balanced purely by stress from elasticity, marks the onset of an elastocapillary regime (Anna & McKinley, 2001; Haward, Sharma, Butts, McKinley, & Rahatekar, 2012). For viscoelastic fluid in the elastocapillary region, the midplane diameter, $D(t)$, decays exponentially according to:

$$\frac{D(t)}{D_1} = \left(\frac{GD_1}{2\sigma}\right)^{1/3} exp[-t/3\lambda_e] \quad (2)$$

where G is elastic modulus and λ_e is the longest relaxation time. The instantaneous strain rate, $\dot{\varepsilon}$, of the thinning fluid filament is given by:

$$\dot{\varepsilon} = -\frac{2}{D(t)}\frac{dD(t)}{dt} \quad (3)$$

Hencky strain, $\varepsilon_H(t)$, experienced by the thinning filament at the axial midplane at time t is then given by:

$$\varepsilon_H(t) = \int_0^t \dot{\varepsilon}(t)d(t) = 2ln\left(\frac{D_1}{D(t)}\right) \quad (4)$$

The apparent transient extensional viscosity (η_e) of the stretching fluid can be obtained using:

$$\eta_e = -\frac{\sigma}{dD(t)/dt} \quad (5)$$

2.8. Statistical analysis

All the experiments were done in triplicate, otherwise specified. Statistical analysis was performed using a one-way analysis of variance (ANOVA) with Duncan post-hoc test at a 95 % confidence level using SPSS software (IBM SPSS Statistics, Version 28.0.1.1(15)).

3. Results and discussion

3.1. Chemical composition

The composition of freeze-dried crude mamaku gum from different

Table 1
Proximate, mineral and simple sugar composition of freeze-dried crude mamaku gum.

	Stage 1	Stage 2	Stage 3
Composition (% w/w dry basis)			
Ash	14.2	23.9	25.0
Protein	5.2	2.2	1.6
Fat	0.5	1.2	2.1
Starch	2.4	1.9	1.3
Sugar	34.6	39.5	47.5
Total dietary fibres	15.5	15.4	18.3
Insoluble dietary fibres	1.6	1.4	1.5
Soluble dietary fibres	13.9	14.0	16.8
Uronic acid	5.8	5.7	6.8
Minerals (mg/kg)			
Potassium	62,217.2	79,382.6	45,209.9
Sodium	4072.4	27,563.4	44,133.5
Calcium	904.9	3528	7642.6
Magnesium	2488.7	1212.8	1937.6
Aluminium	1934.4	2535.8	828.9
Zinc	40.7	71.7	28.0
Manganese	22.3	9.6	10.1
Iron	373.3	374.9	99.1
Copper	14.8	15.6	7.0
Selenium	<0.2	<0.2	<0.2
Lead	0.2	0.2	0.1
Mercury	<0.01	<0.01	<0.01
Sugars (% w/w)			
Fructose	17.9	20.9	21.6
Glucose	16.1	17.9	25.4
Maltose	<0.1	<0.1	<0.1
Sucrose	<0.1	<0.1	<0.1
Galactose	0.68	0.69	0.43

stages is shown in Table 1. All the gum extracts had high proportion of free sugars (stage 1: ~35 %; stage 2: ~40 %; stage 3: ~48 %) and ash (stage 1: ~14 %; stage 2: ~24 %; stage 3: ~25 %). In all extracts, fructose and glucose were the prevalent sugars, while potassium, sodium, calcium, magnesium and aluminium were the predominant minerals. A similarly high ash and sugar content has been shown for extracts from sesame leaves (Nep et al., 2016) and durian seeds (Amid, Mirhosseini, & Kostadinović, 2012). The amount of ash and sugars remarkably increased with the increasing age of mamaku fronds, while the amount of protein was found to be reduced. The extracts were low in fat (stage 1: ~0.5 %; stage 2: ~1 %; stage 3: ~2 %) and starch (stage 1: ~2 %; stage 2: ~2 %; stage 3: ~1 %). About 6–7 % of uronic acid was present in all gum extracts. These results are comparable with the mamaku gum extract composition reported previously (Goh et al., 2007).

Constituent sugar analysis of purified mamaku gum showed that the total sugar content increased with the growth stage (from 57.4 % in stage 1 to 68.5 % in stage 3), although the relative proportions of each of the sugars was similar at each stage (Table 2). The samples contained similar amounts of neutral sugars, mostly galactose, mannose and xylose, as reported previously, but the glucuronic acid content was considerably lower (Wee et al., 2014). However, a comparison of the normalised weight percentage of glucuronic acid (27.4–29.9 %, Table 2) with the relative amounts (mol%) of glucuronic acid linkages (36.1 %) shown by Wee et al. (2014), suggested that the uronic acid content was overestimated in this earlier work. In addition, the relative proportions of glucuronic acid and mannose observed in this current work (~1.2:1) were consistent with a repeating backbone of −4)-β-D-Glc*p*A-(1 → 2)-α-D-Man*p*-(1→, as suggested previously for this and other glucuronomannans (Aspinall, Hirst, & Wickstrøm, 1955; Barone et al., 1996; Erni, Varagnat, Clasen, Crest, & McKinley, 2011; Lai & Liang, 2012; Nep et al., 2016; Wee et al., 2014).

3.2. NMR

The ^{1}H and ^{13}C NMR spectra of purified mamaku gum from each of the three stages were almost indistinguishable from each other (Fig. 1a shows ^{1}H spectra) and were very similar to those obtained previously (Wee et al., 2014). The HSQC spectrum of purified mamaku gum from stage 1 is shown in Fig. 1b; the ^{1}H and ^{13}C chemical shifts were partially assigned on the basis of the HSQC and DFQ-COSY experiments and by comparison with published spectra of similar molecules (Barone et al., 1996; Nep et al., 2016; Wagner et al., 2004; Wagner et al., 2007; Wagner et al., 2008).

Signals at H-1/C-1 5.33–5.37/99.7 ppm, with H-3/C-3 3.74/84.4 ppm were assigned to α-D-Man*p* residues with O-3 substitution, as observed previously by glycosyl linkage analysis (Wee et al., 2014). Similarly, signals at H-1/C-1 4.58/102.9 ppm and 4.53/103.5 ppm were assigned to β-D-Glc*p*A residues, which was confirmed by the presence of a carbonyl signal in the ^{13}C NMR spectrum at 171.5 ppm, and by H-1/H-2 correlations in the DFQ-COSY spectrum with H-2 signals at 3.54 ppm (C-2 74.3 ppm) and 3.39 ppm (C-2 73.5 ppm), respectively. The upfield ^{13}C chemical shift of the GlcA carbonyl signal, together with an intense *O*-methyl signal (^{13}C 54.5 ppm, ^{1}H 3.87 ppm) was consistent with methylesterification of this residue. A signal at H-1/C-1 4.70/104.4 ppm was previously assigned as β-D-Gal*p* (Wee et al., 2014), but correlations in the DFQ-COSY spectrum enabled full assignment of the chemical shifts, which were consistent with β-D-Xyl*p* residues (Sims & Newman, 2006). Signals at H-1/C-1 5.24/101.9 and 5.15/103.0 ppm were assigned to α-D-Gal*p* residues and a weak signal at H-1/C-1 4.90/99.2 ppm was assigned to α-L-Rha*p* residues (H-6/C-6 1.29/17.8 ppm). A signal at H/C 3.44/57.4 ppm suggested that some residues carry a methoxy substituent, such as 3-*O*-methyl rhamnose reported by Barone et al. (1994) for *Ceratozamia spinosa* mucilage.

Table 2
Constituent sugar composition of purified mamaku gum.

Monosaccharide	Amount (wt%)[a]			Normalised (wt%)		
	Stage 1	Stage 2	Stage 3	Stage 1	Stage 2	Stage 3
Fucose	0.8	0.6	0.7	1.5	1.0	1.0
Rhamnose	1.2	1.6	1.4	2.1	2.6	2.0
Arabinose	2.1	2.2	2.7	3.6	3.7	4.0
Xylose	5.7	5.9	6.6	9.9	9.7	9.6
Galactose	15.0	17.0	18.4	26.2	27.6	26.9
Glucose	2.6	0.6	1.8	4.6	1.0	2.7
Mannose	13.8	14.9	16.5	24.0	24.2	24.1
Galacturonic acid	0.5	0.2	0.4	0.8	0.3	0.5
Glucuronic acid	15.8	18.4	20.0	27.4	29.9	29.2
Total	57.4	61.4	68.5	100.0	100.0	100.0

[a] Values are the average of duplicate analyses (n = 2).

3.3. Size-exclusion chromatography coupled with multi-angle laser light scattering (SEC-MALLS)

Fig. 2 shows the chromatogram for purified mamaku gum from different stages at an elution time ranging between 20 and 30 min. A right-hand shift in eluting time can be observed with increasing age. M_w and R_z significantly decreased with an increase in age; M_w decreased from ~4.1 × 10^6 Da to ~2.1 × 10^6 Da while R_z decreased from ~147 nm to ~108 nm from stage 1 to stage 3, respectively (Table 3). These results are consistent with Goh, Matia-Merino, Pinder, Saavedra, and Singh (2011) who reported M_w = ~3.2 × 10^6 Da and R_z = ~144 nm for mamaku gum extracted from a mix of stage 1 and stage 2 fronds. On the other hand, Wee et al. (2014), reported M_w = ~2 × 10^6 Da and R_z = ~94 nm for mamaku gum extracted from a similar age mix fronds. The differences in these molecular parameters could be due to differences in frond maturity, harvesting season, sample preparation (heating at high temperature and ethanol precipitation) and/or differences in instrumental parameters (different analytical columns and mobile phase were used). Further, our results showed a shift from a monomodal peak to a bimodal peak (for the stage 3 gum) with increasing harvesting age (Fig. 2). This shift in peaks profile was also accompanied by a significant increase in polydispersity index (M_w/M_n). These results suggest that MP undergoes (enzymatic) hydrolysis with the increase in frond maturity which may result in various molecular weight sizes of the polysaccharide. The hydrolysis of polysaccharides with plant ageing is a common phenomenon. There is a variety of enzymes such as *β*-glucosidase, *α*-glucosidase, *β*-mannanase, galacturonanase, *β*-1,3-glucanase, galactanase and *β*-xylosidase present in plants that are capable of hydrolysing most of the glycosidic bonds in the polysaccharides (Franková & Fry, 2013). In seeds like guar and locust, galactomannan is the main endosperm carbohydrate that is hydrolysed by enzymes such as 1,4-*β*-mannan hydrolase, *β*-mannosidase, and *α*-galactosidase during germination (McCleary & Matheson, 1974; Reid & Meier, 1973). However, further work is needed to identify enzymes specific to the hydrolysis of MP.

3.4. Shear rheology

Shear rheology was performed to quantify the flow behaviour of the gums from the three different harvesting age stages. The viscosity profiles of crude mamaku gum (1 %, 3 %, 5 % and 10 % w/w total solids) extracted from the three stages are shown in Fig. 3. Mamaku gum from stages 1 and 2 exhibited the unique rheological behaviour with three different regions—Newtonian region at the low shear rate, followed by a region of shear-thickening at intermediate shear rates, and shear-thinning at higher shear (Fig. 3a, b). With the increase in gum concentration for both of these samples (stage 1 and 2), the viscosity increased across the whole shear rate range and the rate at the onset of shear-thickening (critical shear rate- $\dot{\gamma}_{crit}$) shifted to lower shear rates (stage 1: from 6.31 s^{-1} at 3 % w/w to 2 s^{-1} at 5 % w/w; stage 2: from 7.94 s^{-1} at 3 % w/w to 2.51 s^{-1} at 5 % w/w). The shear-thickening in MP has

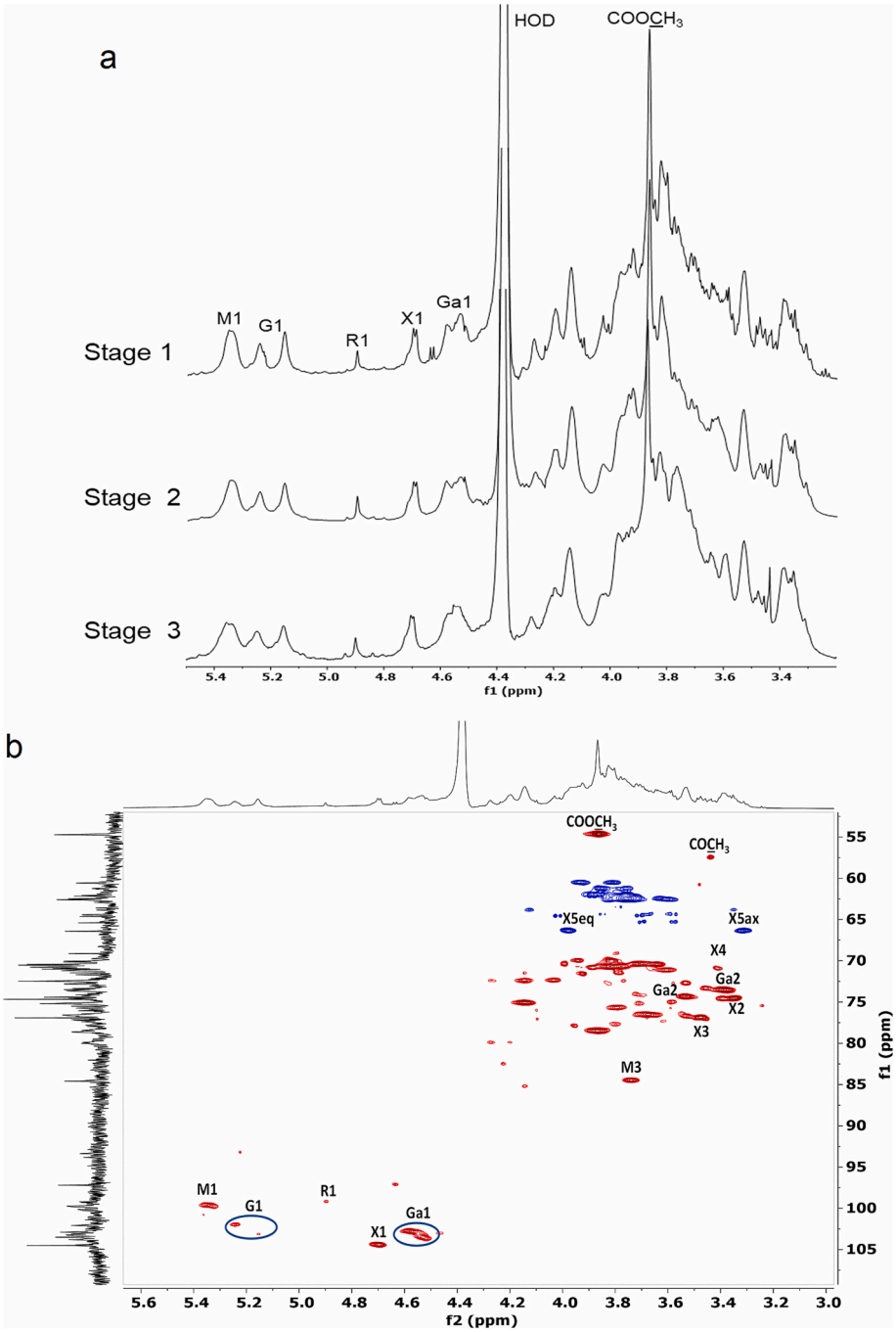

Fig. 1. (a) Selected region of ^{1}H spectra of purified mamaku gum. (b) Selected region of DEPT-edited HSQC spectrum of purified mamaku gum from stage 1. M, mannose; G, galactose; R, rhamnose; X, xylose; Ga, glucuronic acid; COOCH$_3$, methylesterification at C-6; COCH$_3$, *O*-methoxy group.

been proposed to be due to the unfolding of polymer chains and breaking of intramolecular bonds with increasing shear rate, leading to the formation of intermolecular hydrogen bonds with neighbouring polymer chains (Wee, Matia-Merino, & Goh, 2015). When the mamaku gum concentration is increased, an increase in chain-chain interactions including physical entanglements of the polymer chains is expected. This will lead to an overall increase in viscosity and the corresponding decrease in $\dot{\gamma}_{crit}$. The shift to a lower $\dot{\gamma}_{crit}$ implies that the polymer rheological properties are more dependent on the shear. In the case of the mamaku gum, a high gum concentration (or lower $\dot{\gamma}_{crit}$) implies that a lower shear rate is needed to induce the shear thickening behaviour.

Despite similar viscosity profiles for stage 1 and stage 2 gum samples, two key differences were observed (Table A2); (i) The viscosity developed by the gum from stage 1 was higher than that from stage 2 at all ranges of applied shear. When comparing at 5 % (w/w) total solids, the gums from stage 1 and stage 2 had similar uronic acid content (~0.3 %) but the maximum viscosity (η_{max} -at the peak) for stage 1 gum was markedly higher, ~4.2 Pa.s (at 12 s^{-1}) compared to the η_{max} for stage 2 gum, ~1.4 Pa.s (at 13 s^{-1}) (Fig. 3d). From this, it is obvious that the difference in viscosity between the two stages is not due to any changes in the uronic acid content (Fig. A2); (ii) The extent of shear-thickening, defined as the ratio between the peak viscosity during shear-thickening and the viscosity at the onset of shear-thickening (η_{max}/η_{crit}), was higher for stage 2 gum than for stage 1. For instance, at 3 % and 5 % (w/w), the extent of shear-thickening for stage 2 gum was ~4.1 and ~3.9, respectively, while it was ~3.5 and ~3.3, respectively, for stage 1 gum.

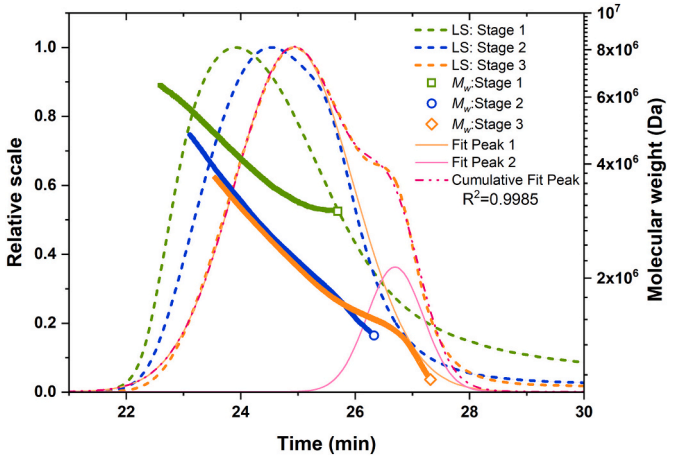

Fig. 2. Light scattering (LS) signal and weight-average molar mass (M_w) analysis by size-exclusion chromatography coupled with multi-angle laser light scattering (SEC-MALLS) of purified mamaku gum. The two peaks for the stage 3 gum sample were deconvoluted using the Gaussian model (R^2 = 0.999) in Origin 2020 (Version 9.7.0.185 Academic).

Table 3
Molecular parameters of purified mamaku gum analysed by Size-exclusion chromatography coupled with multi-angle laser light scattering (SEC-MALLS).

	Weight-average molar mass, M_w ×10^6 (Da)	Root mean square radius, R_z (nm)	Slope from the plot of M_w against root-mean-square radius	Polydispersity (M_w/M_n)
Stage 1	4.07 ± 0.16[a]	146.45 ± 3.58[a]	0.68 ± 0.01[a]	1.05 ± 0.01[b]
Stage 2	2.61 ± 0.02[b]	123.15 ± 1.08[b]	0.61 ± 0.01[b]	1.14 ± 0.01[a]
Stage 3	2.09 ± 0.02[c]	107.88 ± 1.31[c]	0.6 ± 0.01[b]	1.11 ± 0.0[a]

Values are expressed as means ± standard deviation (n = 3). Values in the same column denoted with the different superscripts are significantly different ($p \leq 0.05$).

Contrary to stages 1 and 2 gums, no shear-thickening was observed for the gum from stage 3, even at a high concentration of 10 % (w/w) (corresponding to ~0.65 % uronic acid) (Fig. 3c). Furthermore, stage 3 gum had the lowest viscosity at all shear rates amongst all three gum samples (Fig. 3d).

Crude mamaku gum from different stages of harvesting age was also subjected to frequency sweep at 5 % strain- within the linear viscoelastic region (Fig. 4). Storage (G') and loss moduli (G'') increased for all samples with increasing frequency and concentration. At low frequencies, G'' was above G' for all three samples, indicating a viscous flow behaviour, meaning that MP chains can relax to the original equilibrium configuration within the time scale. With an increase in frequency, for stage 1 and stage 2 gums at 5 % and 10 % (w/w), G′ became dominant over G'' above the crossover frequency ($G' = G''$) (Fig. 4a, b). G' greater than G'' indicates a change from viscous to 'gel-like' behaviour. The inverse of frequency at the crossover point is the relaxation time (λ_s). With the increase in concentration, the λ_s increased from 0.32 s at 5 % to 20 s at 10 % for stage 1 gum and from 0.12 s to 4 s for stage 2 (Table A3). The higher λ_s for stage 1 gum compared to stage 2, suggest that polymer chains in the stage 1 gum form a stronger network of inter- and intra-molecular interactions (hydrogen bonding), thus, taking longer to relax. For stage 3 gum, G'' remained higher than G' for all the concentrations, indicating viscous fluid behaviour, due to limited polysaccharide linkages (Fig. 4c). Similar to the viscosity trend observed above, G' and G'' decreased with an increase in the harvesting age, at a given frequency, as stage 1 > stage 2 > stage 3.

3.5. Extensional rheology

Fig. 5 shows the sequence of images demonstrating the filament thinning dynamics as a function of time for crude gum samples from stage 1, stage 2 and stage 3 at 3 % and 5 % (w/w) total solids concentrations. The time in Fig. 5 is normalised by t_b, *i.e.*, $t' = t/t_b$ (t_b values are given in Table A1). $t' = 0$ is the instant when piston stretching ceases and corresponds to the starting time point of the experiment. Soon after the liquid bridge has been formed, the inertial stresses arising due to displacement of the piston are dominant (inertial regime). This is immediately followed by the viscocapillary regime, where capillary forces are balanced by the viscosity of the fluid. The filament diameter in the viscocapillary regime decreases linearly according to Eq. (1) (McKinley & Tripathi, 2000). Following the viscocapillary regime, is the exponential elastocapillary regime where filament diameter decays as D (t) ~ exp(−t/3 λ_e) (from Eq. (2)) (Entov & Hinch, 1997). The onset of the elastocapillary regime can be viewed in images in Fig. 5 (marked in-dash-boxes), characterised by the presence of a stable axially uniform cylindrical fluid filament that thins with time. Mamaku gum from stage 1 and stage 2 enters into the elastocapillary regime faster than in stage 3. With the increase in concentration, the liquid bridge can sustain a thinner fluid filament without breaking; for example, for stage 2 gum, at $t' = 0.65$, the filament diameter decreases with an increase in concentration—attributing to higher elastic stress at 5 % (w/w) concentration that retards the breakup. Towards the breakup stage, the polymer chains become fully stretched and the elastic stress can no longer balance the increasing capillary stress, the filament behaves like a viscous Newtonian fluid and the diameter will decay linearly until breakup (Entov & Hinch, 1997). In order to predict the evolution of diameter in both the elastocapillary and long-time viscous-like regimes, Anna and McKinley (2001) proposed a generalised form of Eq. (2) as:

$$D(t) = Ae^{-Bt} - Ct + D \quad (6)$$

where A, B, C and D are fitting parameters. The value of B is related to the longest extensional relaxational time (λ_e) of the fluid (B = 1/3λ_e), and the value of C is related to the steady-state extensional viscosity plateau at larger Hencky strains (C = $\sigma/\eta_{e,\infty}$).

The evolution of fluid filament diameter with time is shown in Fig. 6. The decrease in filament diameter follows an exponential decay, characteristic of polymer fluids as reported previously for guar gum (Bourbon et al., 2010; Kongjaroen, Methacanon, & Gamonpilas, 2022; Piermaría, Bengoechea, Abraham, & Guerrero, 2016; Szopinski et al., 2016; Torres, Hallmark, & Wilson, 2014), xanthan (Choi, Mitchell, Gaddipati, Hill, & Wolf, 2014; Funami & Nakauma, 2021), mamaku (Jaishankar et al., 2015), locust bean gum (Bourbon et al., 2010; Funami & Nakauma, 2021; Piermaría et al., 2016), polystyrene (Clasen et al., 2006; Vadillo, Mathues, & Clasen, 2012) and polyelectrolyte solutions (Jimenez, Dinic, Parsi, & Sharma, 2018). For mamaku gum extracted from different harvesting ages, t_b increased with an increase in concentration, indicating enhanced entanglement/interactions between stretched polymer chains in a concentration-dependent manner. At a given concentration, filament formed by stage 2 gum took the longest time to break (maximum t_b) while the breakup was fastest for stage 3 gum (minimum t_b). From the filament diameter *vs* time plot, using Eq. (2) in the elastocapillary regime, λ_e was calculated and values are given in Fig. 6 and Table A1. On comparing λ_e, stage 2 gum has higher λ_e followed by stage 1 and then stage 3 gum; at 5 % (w/w) λ_e was 6.8 s, 3.2 s and 0.2 s respectively.

The relaxation time of a polysaccharide is related to the time taken by the polysaccharide chains to reach an equilibrium state after being disturbed. In this study, λ_s and λ_e were determined from oscillatory shear rheology and filament thinning diameter, respectively, and are given in Tables A1 and A3. At 5 % (w/w) mamaku gum concentration for stage 1 and stage 2, λ_e was above λ_s. Similar observations, $\lambda_e > \lambda_s$, were made by Vadillo et al. (2012) and Clasen et al. (2006) for different molecular

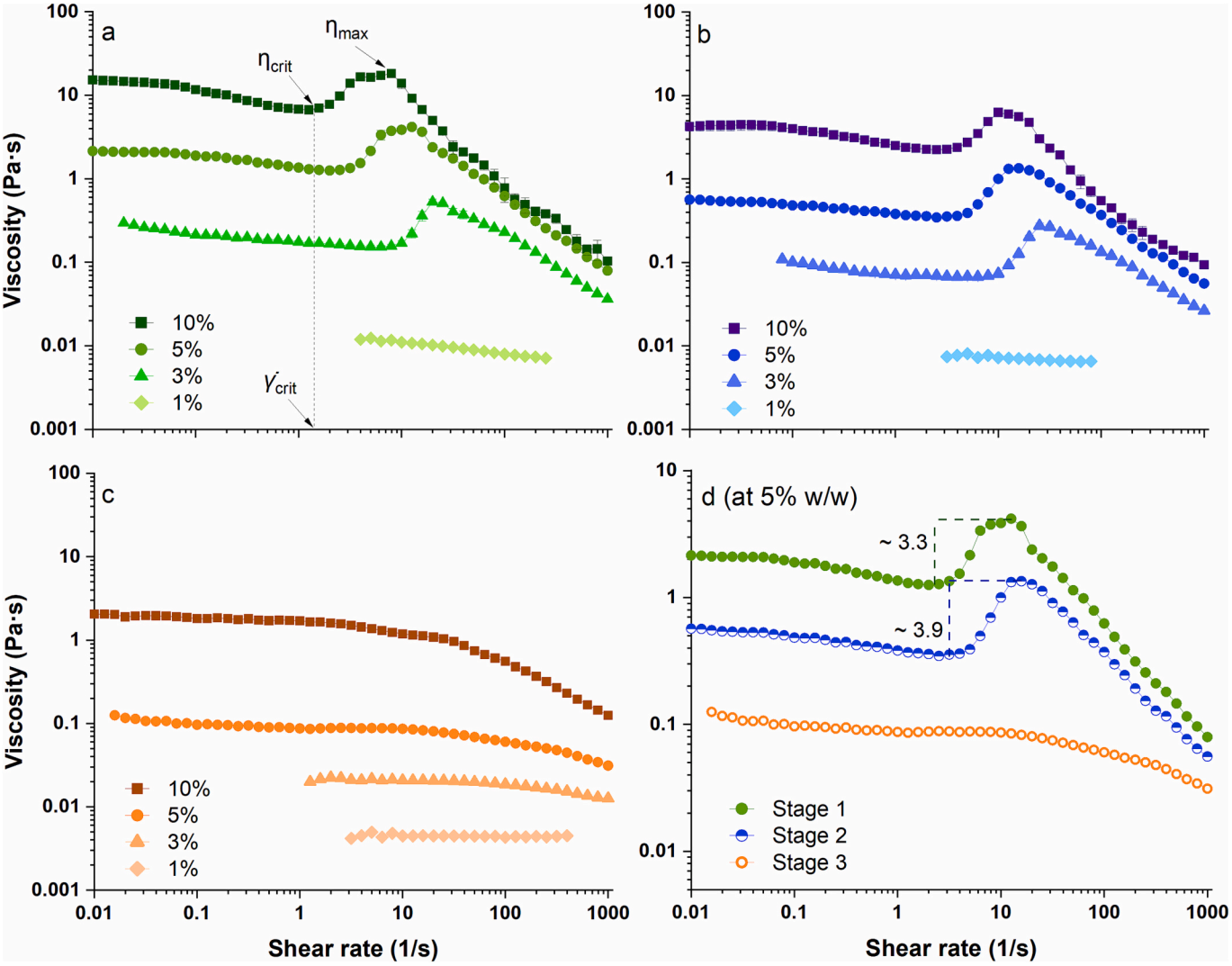

Fig. 3. Viscosity profiles of mamaku gum extracted from (a) stage 1, (b) stage 2 and (c) stage 3 as a function of shear rate. (d) Comparison of viscosity for mamaku gum extracted at 5 % (w/w total solids), marked with η_{max}/η_{crit} ratios. Values are plotted as means ± standard deviation (n = 3). Measurements were taken using cup-and-bob geometry at 20 °C. η_{max}, maximum viscosity (Pa.s); $\dot{\gamma}_{crit}$, critical shear rate (s^{-1}); η_{crit}, critical viscosity (Pa.s); η_{max}/η_{crit}, extent of shear-thickening.

weight polystyrene solutions and by Szopinski et al. (2016) for carboxymethyl hydroxypropyl guar gum solution. On the contrary, Anna and McKinley (2001) demonstrated that $\lambda_e \approx \lambda_s$ for Boger fluids, while Yesilata, Clasen, and McKinley (2006) and Arnolds, Buggisch, Sachsenheimer, and Willenbacher (2010) showed $\lambda_e < \lambda_s$ for wormlike micelle solution based on erucyl bis(2-hydroxyethyl) methyl ammonium chloride (EHAC) and for poly(ethylene oxide) (PEO) solutions, respectively. The possible reason for the difference in λ_e and λ_s could be due to the difference in the mode of relaxation for shear and extensional flows. During extensional deformation, a single polysaccharide coil deforms and λ_e refers to the disentanglement of the entire polymer chain (Clasen et al., 2006; Szopinski et al., 2016). Whereas under shear deformation, polysaccharide chain movements can be dominated by entanglements and λ_s refers to the time that a disentangled polymer requires to re-entangle with the neighbouring polymer molecules (Kongjaroen et al., 2022). In the case of mamaku, the possible reason for $\lambda_e > \lambda_s$ could be the more stretched MP under extensional flow—more sites for hydrogen bonding leading to greater intermolecular interactions—compared to partly stretched chains under oscillatory flow. During extensional behaviour, polymers are significantly stretched as they approach the elastocapillary regime, and they are further stretched as the filament evolves until a fully stretched polymer is achieved, thus, making intermolecular interactions significant, causing higher λ_e (Tirtaatmadja, McKinley, & Cooper-White, 2006). Interestingly, Bhardwaj, Miller, and Rothstein (2007), reported a concentration-dependent change in λ_e/λ_s for wormlike micelle solutions of cetylpyridinium chloride and sodium salicylate (NaSal) and cetyltrimethylammonium bromide and NaSal; at low concentration, λ_e was lower than λ_s, while at higher concentration λ_e was above λ_s. Mamaku concentration of 5 % (w/w) is above the coil overlap concentration ($c^* = 2.2$ % (w/w) (Goh et al., 2007) so, $\lambda_e > \lambda_s$ for mamaku gum could also be a concentration effect, as λ_e is reported to be more sensitive to concentration than λ_s (Bhardwaj et al., 2007; Clasen et al., 2006; Tirtaatmadja et al., 2006). Since no crossover was observed at 1 % and 3 % concentrations from oscillatory data, λ_s was not determined and no comparison between λ_e and λ_s was made at lower concentrations.

The elastocapillary balance persists for sufficient time for stage 1 and stage 2 gum samples at 3 % and 5 % (w/w) concentration, thus, 3 % and 5 % (w/w) concentrations were used to estimate apparent transient extensional viscosity, η_e, as a function of accumulated Hencky strain, $\varepsilon_H(t)$. A marked increase in η_e was observed for both sample types as $\varepsilon_H(t)$ increases in a concentration-dependent manner; ultimately reaching a plateau due to the molecules reaching their finite extensibility limit (Fig. 6d). Similar to λ_e trend, η_e was higher for the gum from

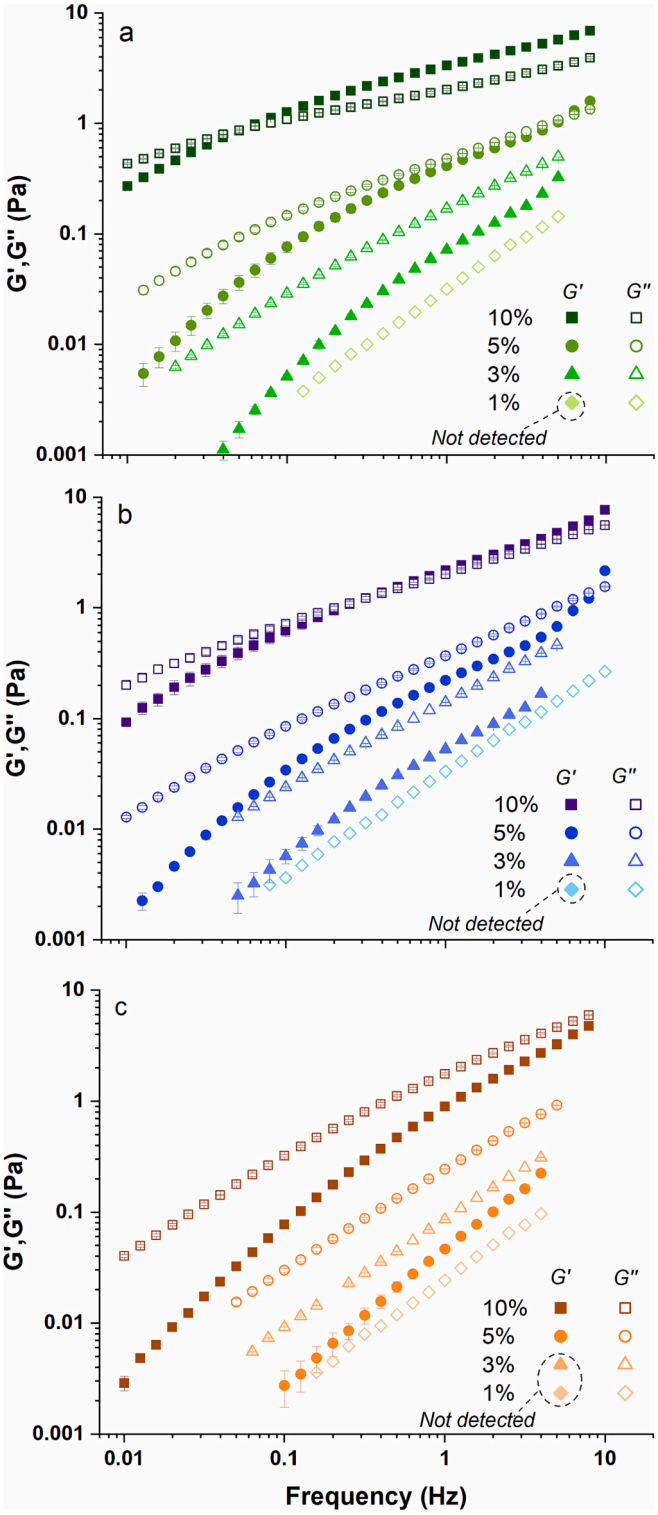

Fig. 4. Storage modulus (G', filled symbols) and loss modulus (G'', empty symbols) of mamaku gum extracted from (a) stage 1, (b) stage 2 and (c) stage 3 at 1 %, 3 %, 5 % and 10 % w/w total solids as a function of frequency. Oscillatory measurements (frequency sweep) were performed in the range of 0.01–20 Hz using a constant strain value of 5 % (within the linear viscoelastic region) using the double gap geometry (DG-26-7 and C-PTD 200) at 20 °C. Values are plotted as means ± standard deviation (n = 3).

stage 2 than from stage 1, suggesting stronger extensional behaviour for the former. For both stage 1 and 2 gum, the η_e is considerably higher (η_e > 200 Pa.s) than other polymers such as guar gum (η_e < 10 Pa.s) (Torres et al., 2014), hydroxypropyl ether guar gum (η_e < 10 Pa.s) (Duxenneuner, Fischer, Windhab, & Cooper-White, 2008), and okra polysaccharide (η_e < 100 Pa.s) (Yuan et al., 2018). Also, $\eta_e \gg \eta_s$ suggests that MP exhibits a more dramatic response to extensional deformation compared to shear deformation as the association of MP chains is strengthened in extensional flow since the polymer is more stretched.

4. General discussion

MP is a negatively charged biomacromolecule with unique rheological properties. Herein we showed that the rheological behaviour of MP is dependent on the harvesting age of the mamaku fronds. The molecular weight (chain-length) of MP decreases (Fig. 2 and Table 3), with increasing harvest age without any apparent alteration in chemical structure (Fig. 1 and Table 2). The harvesting-age-dependent decrease in chain length of MP leads to a reduction in viscosity at all shear rates ($\eta_{s\text{-}Stage\ 1} > \eta_{s\text{-}Stage\ 2} > \eta_{s\text{-}Stage\ 3}$, Fig. 3d). A similar molecular weight-dependent decrease in viscosity was observed previously for xanthan gum (Holzwarth, 1978), guar gum (Beer, Wood, & Weisz, 1999) and starch (Iida, Tuziuti, Yasui, Towata, & Kozuka, 2008).

Despite MP from stage 1 having a higher molecular weight than that from stage 2, t_b, λ_e and η_e were greater for the latter (Fig. 6). Furthermore, the trend for extensional behaviour is similar to the ratio η_{max}/η_{crit}, observed in shear rheology (stage 2 > stage 1) (Fig. 3d). For extensional rheology, in general, t_b, λ_e and η_e increase with an increase in molecular weight (Anna & McKinley, 2001; Wunderlich et al., 2000). However, for polymers with complex architecture, the extensional behaviour can also be influenced by additional structural parameters like the rigidity of the backbone and the degree and length of branching, which can influence the interaction between the polymer chains. For example, in the case of polymer melts, the extensional behaviour was reported to be more pronounced for long-chain-branched polymer melts than linear polymer melts—explained by an increase in resistance to flow by the side branches after reaching a certain chain length sufficient for intermolecular entanglements (Vasilyev, Dreval, Malkin, & Kulichikhin, 2010; Wagner et al., 2000), and/or the ability of branches to distribute the stress into material leading to longer relaxation time (Kasehagen & Macosko, 1998). In this study, there was no difference in the chemical structure of the polysaccharide extracted from different harvesting ages, but only the size of the polysaccharide.

The observed behaviour suggests greater intermolecular interactions between polymer chains from stage 2 than in stage 1. The presence of high protein (~5.2 % *w*/w dry bases, Table 1) in the stage 1 sample may interfere with the intermolecular interactions between MP chains, resulting in lower η_{max}/η_{crit}, t_b, λ_e and η_e, than stage 2 sample. Simultaneously, the difference in the ash content of stage 1 and stage 2 extracts (Table 1), resulting in different ionic strengths of ~14.8 mM and ~23 mM, respectively, might affect the screening of negative charges on MP. Wee et al. (2015) reported that MP is very sensitive to the ionic strength of the system, especially at concentrations below 200 mM. With increasing ionic strength, intramolecular repulsion within the MP chains reduces, making them less extended, therefore decreasing viscosity. Thus, we tested the effect of ionic strength on the viscosity of the stage 1 sample. The ionic strength of the stage 1 sample was increased to match the ionic strength of stage 2 sample by adding NaCl or $CaCl_2$. A decrease in the viscosity at low shear rates (0.01–1 s^{-1}) was observed (Fig. 7); η_{crit} reduced on increasing ionic strength without affecting η_{max}, thereby increasing the η_{max}/η_{crit} (~3.9). The increased η_{max}/η_{crit} for stage 1 after adding salts was comparable to the native stage 2 sample. However, at similar ionic strength, one would expect higher η_{max}/η_{crit} for longer MP chains from the stage 1 sample, thus, the difference in ionic strength alone cannot explain the observed behaviour. Additionally, there may be a critical chain length of the polysaccharide where maximum

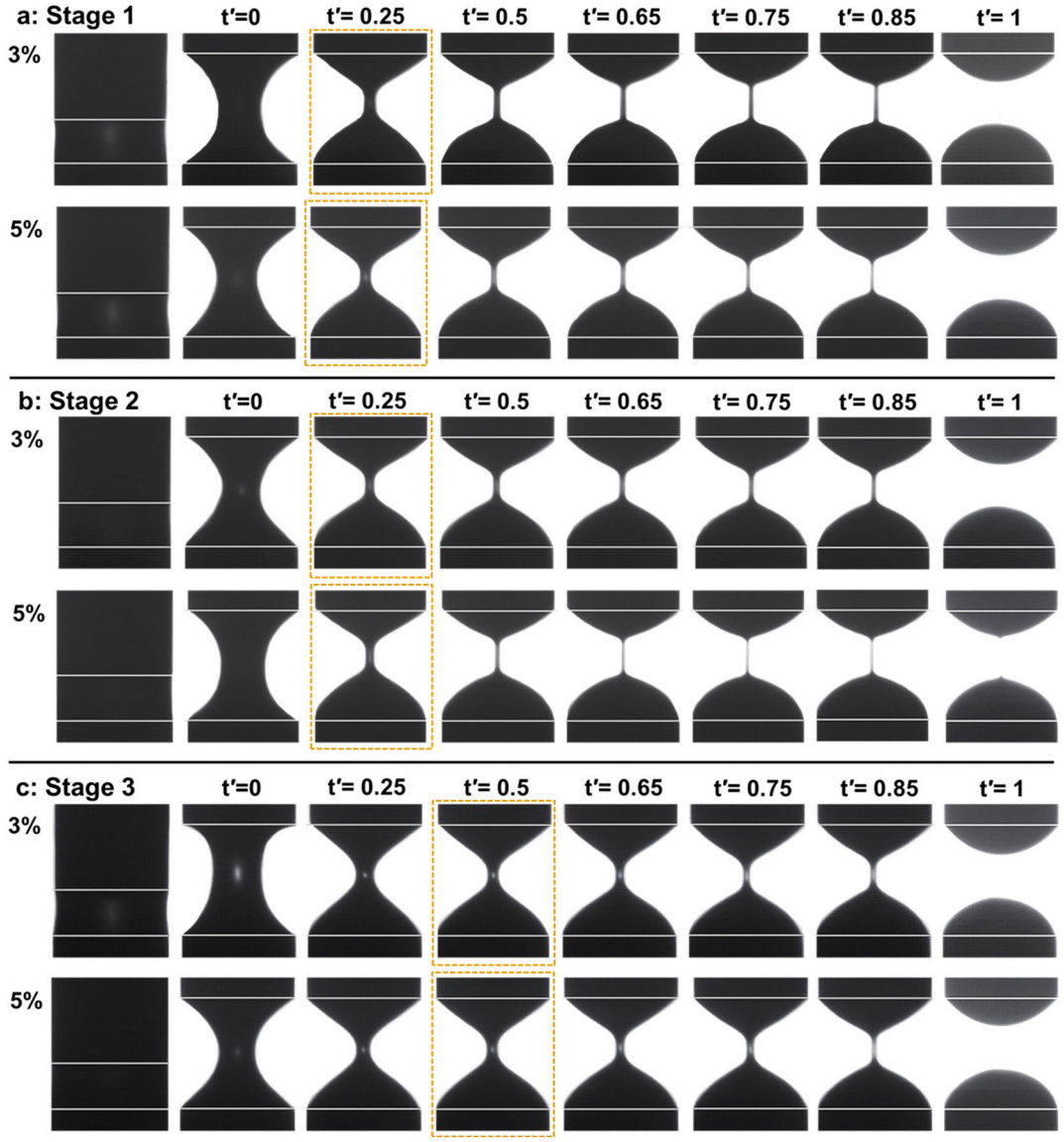

Fig. 5. Still images of the fluid filament during uniaxial extensional rheology experiment for mamaku gum from (a) stage 1, (b) stage 2 and (c) stage 3 as a function of time. The onset of the elastocapillary regime, characterised by a uniform fluid filament, is marked in-dash-boxes. The time is normalised by t_b, *i.e.*, $t' = t/t_b$ (capillary breakup time, t_b, values are given in Table A1). The initial gap is $L_o = 1.5$ mm, the final gap $L_f = 4$ mm and the piston diameter $D_o = 4$ mm, giving initial and final aspect ratios of $\Lambda_o = 0.38$ and $\Lambda_f = 1$, respectively.

intermolecular hydrogen bonding is achieved, resulting in stronger shear-thickening and extensional behaviours. The polysaccharide chains from stage 2 fronds, upon shearing/stretching, may unfold completely by disrupting intramolecular bonds. This will expose a greater number of associative groups, leading to the formation of intermolecular hydrogen bonding (Fig. 8b). As the chain length increases above the critical length (in the case of stage 1), the intramolecular interactions per chain may also increase, which may limit the unfolding of the chains upon shearing/stretching. Thus, limiting the exposure of associative groups can result in reduced intermolecular interactions than for the shorter chain lengths of MP from stage 2 (Fig. 8a). On the contrary, as the chain length decreases below the critical length, the polymer chains are likely to unfold completely upon shearing/stretching, however, the shear-thickening and extensional behaviours may reduce due to a decrease in the number of sites for intermolecular interaction. As the chain length decreases further, beyond a certain limit, there may be no intermolecular interaction between MP chains to cause shear-thickening behaviour as observed in the stage 3 MP (Fig. 8c).

Interestingly, with the increase in the concentration of MP, the η_{max}/η_{crit} decreases and the difference between η_{max}/η_{crit} for the polymers from stage 1 and stage 2 reduces—at 10 % (w/w) η_{max}/η_{crit} was ~2.7 for both gum samples (Table A2). The reduction in η_{max}/η_{crit} could be attributed to a decrease in free volume with an increase in concentration, which may limit the unfolding of MP chains and consequently, intermolecular interactions. On the other hand, the difference in extensional behaviour for stage 1 and stage 2 samples becomes more pronounced with an increase in concentration (Fig. 6 and Table A1). In addition to chain length, the extensional behaviour may also be affected by the number of polymer chains. At a given concentration of gum from stage 1 and stage 2, the gum from stage 2 will have a higher number of polymer chains —because of its smaller size—thus, have more load-bearing strands, which can result in stronger extensional behaviour when compared to stage 1 gum (Liu et al., 2013).

5. Conclusions

This study shows the age-dependent decrease in the molecular weight of the MP as the fronds mature, which impacted the shear and

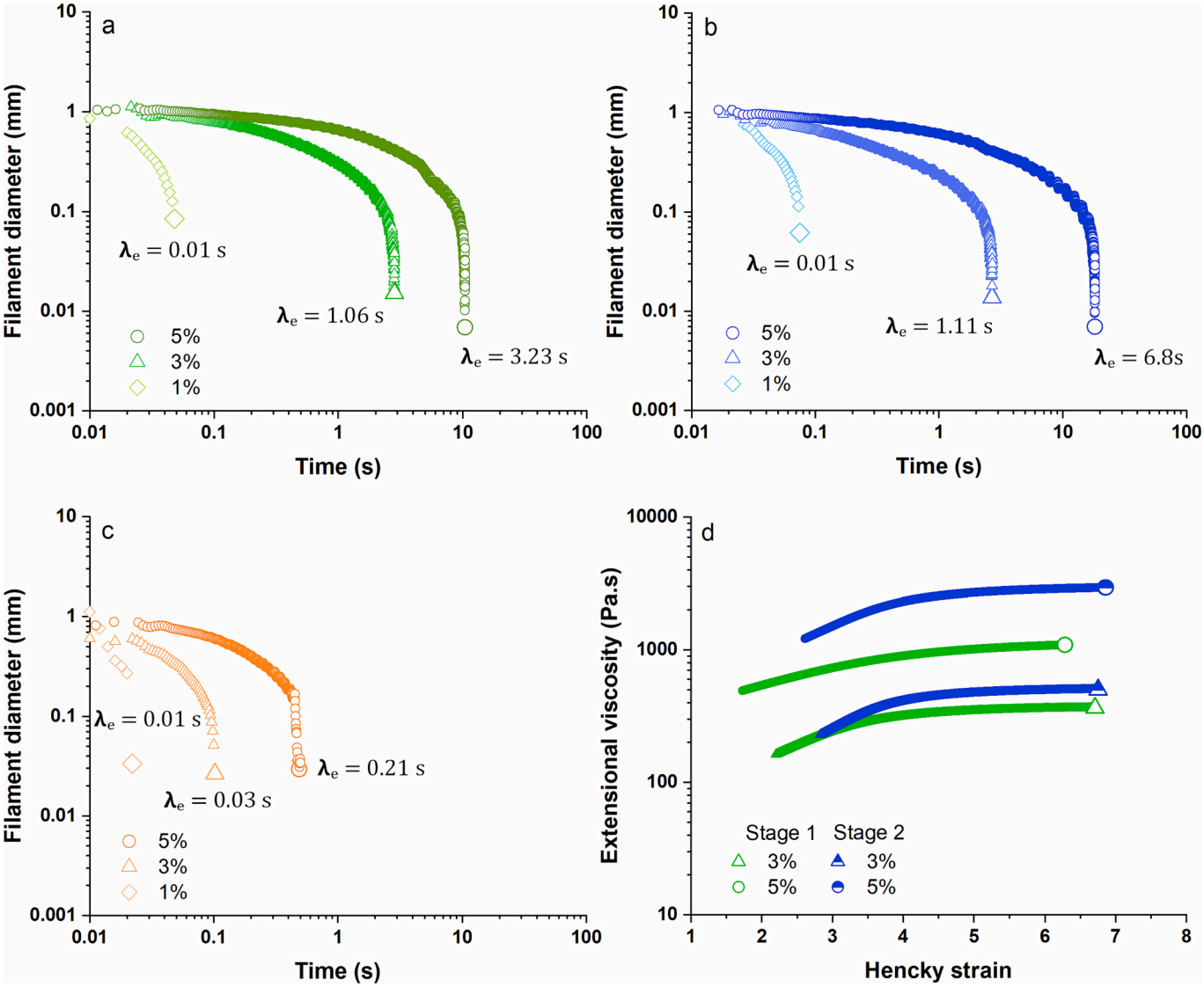

Fig. 6. Dynamics of midfilament diameter as a function of time for mamaku gum extracted from (a) stage 1, (b) stage 2 and (c) stage 3. (d) Transient extensional viscosity of mamaku gum from stages 1 and 2 as a function of Hencky strain.

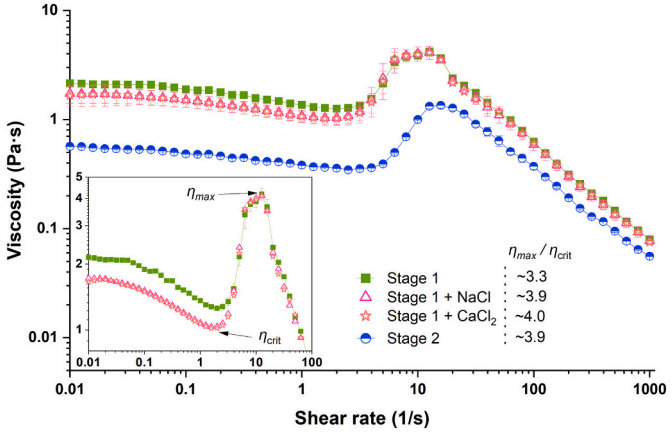

Fig. 7. Viscosity profile of mamaku gum (5 % w/w) from stage 1 after altering ionic strength by adding NaCl and $CaCl_2$. Native stage 1 and stage 2 mamaku gum (5 % w/w) are added for reference.

extensional behaviours, thus, confirming our original hypothesis. Based on these results, young and fully grown fronds may be harvested to extract MP—with retained shear-thickening behaviour and longer capillary breaking time than MP from senescent (dying) fronds—for commercial applications such as in the cosmetic, pharmaceutical, petroleum and food industries. Further work on the sensitivity of MP to industrial operations such as temperature, shear and pressure, which are critical during the processing of MP for commercial applications, is underway. The final aim is to use MP as an ingredient in food systems targeting safe swallowing, satiety management, and improved colon health.

Funding

The research was funded by the High-Value Nutrition programme of The New Zealand National Science Challenges in the program *Mamaku whakaoraora* (Contract no. AUAX1902). The New Zealand Institute for Plant and Food Research Limited funded Akshay's PhD studies (PFR Contract no. 38041).

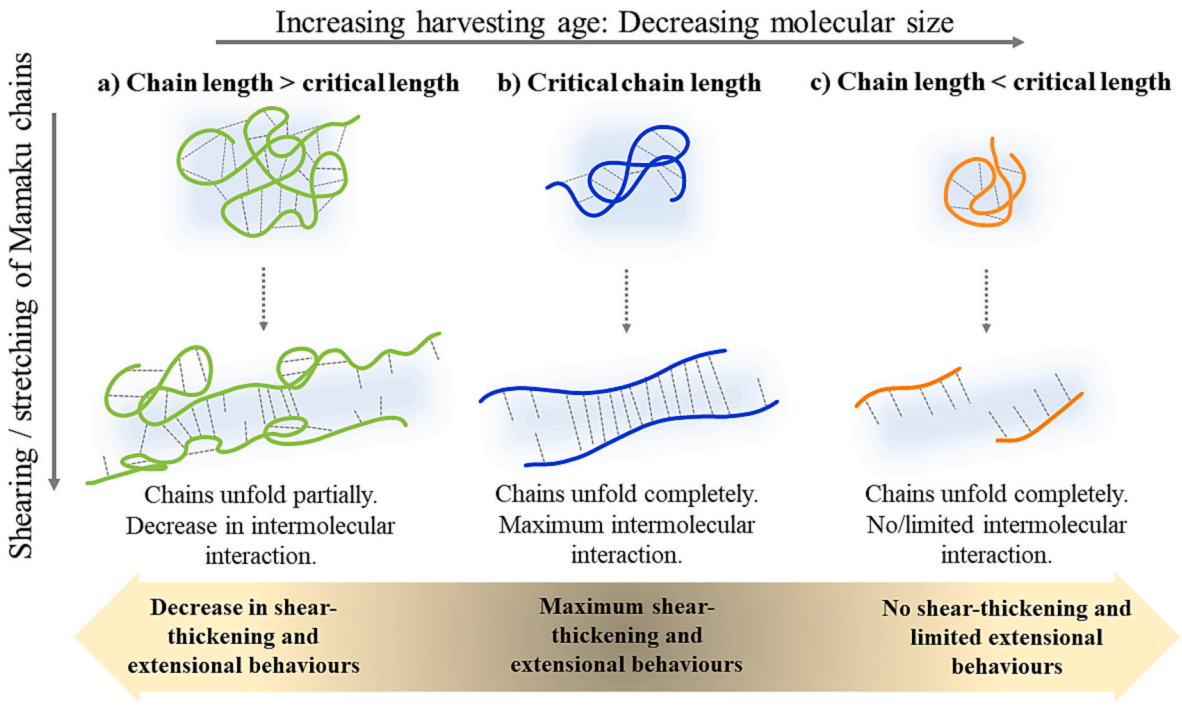

Fig. 8. Schematic illustration showing the unfolding of mamaku polysaccharide chains from (a) stage 1, (b) stage 2 and (c) stage 3 on shearing or stretching and influence on intermolecular hydrogen bonds with neighbouring chains.

CRediT authorship contribution statement

Akshay Bisht: Conceptualization, Formal analysis, Investigation, Methodology, Validation, Visualization, Writing – original draft. **Kelvin K.T. Goh:** Conceptualization, Methodology, Supervision, Writing – review & editing. **Ian M. Sims:** Investigation, Writing – original draft. **Patrick J.B. Edwards:** Investigation, Writing – review & editing. **Lara Matia-Merino:** Conceptualization, Methodology, Project administration, Supervision, Writing – review & editing.

Declaration of competing interest

The authors declare that they have no known competing financial interests or personal relationships that could have appeared to influence the work reported in this paper.

Data availability

Data will be made available on request.

Acknowledgement

The project was consulted with Prof. Dr. Nicholas Rahiri Roskruge (from the Māori leadership team, College of Science at Massey University) for cultural review and Mātuaranga Māori.

Appendix A. Supplementary data

Supplementary data to this article can be found online at https://doi.org/10.1016/j.carbpol.2023.121757.

References

Amid, B. T., Mirhosseini, H., & Kostadinović, S. (2012). Chemical composition and molecular structure of polysaccharide-protein biopolymer from Durio zibethinusseed: Extraction and purification process. *Chemistry Central Journal, 6*(1), 1–14.

Ang, C. L., Goh, K. K. T., Lim, K., & Matia-Merino, L. (2021). Rheological characterization of a physically-modified waxy potato starch: Investigation of its shear-thickening mechanism. *Food Hydrocolloids, 120*, Article 106908.

Anna, S. L., & McKinley, G. H. (2001). Elasto-capillary thinning and breakup of model elastic liquids. *Journal of Rheology, 45*(1), 115–138.

Arnolds, O., Buggisch, H., Sachsenheimer, D., & Willenbacher, N. (2010). Capillary breakup extensional rheometry (CaBER) on semi-dilute and concentrated polyethyleneoxide (PEO) solutions. *Rheologica Acta, 49*(11), 1207–1217.

Aspinall, G. O., Hirst, E. L., & Wickstrøm, A. (1955). Gum ghatti (Indian gum). The composition of the gum and the structure of two aldobiouronic acids derived from it. *Journal of the Chemical Society*, (0), 1160–1165.

Barone, G., Corsaro, M. M., De Castro, C., Lanzetta, R., Mangoni, L., & Parrilli, M. (1994). Structural investigation of *Ceratozamia spinosa* mucilage. *Carbohydrate Research, 260*(2), 259–270.

Barone, G., Corsaro, M. M., Giannattasio, M., Lanzetta, R., Moscariello, M., & Parrilli, M. (1996). Structural investigation of the polysaccharide fraction from the mucilage of *Dicerocaryum zanguebaricum* Merr. *Carbohydrate Research, 280*(1), 111–119.

Beer, M. U., Wood, P. J., & Weisz, J. (1999). A simple and rapid method for evaluation of Mark–Houwink–Sakurada constants of linear random coil polysaccharides using molecular weight and intrinsic viscosity determined by high performance size exclusion chromatography: Application to guar galactomannan. *Carbohydrate Polymers, 39*(4), 377–380.

Bhardwaj, A., Miller, E., & Rothstein, J. P. (2007). Filament stretching and capillary breakup extensional rheometry measurements of viscoelastic wormlike micelle solutions. *Journal of Rheology, 51*(4), 693–719.

Bisht, A., Goh, K. K., & Matia-Merino, L. (2023). The fate of mamaku gum in the gut: Effect on in vitro gastrointestinal function and colon fermentation by human faecal microbiota. *Food & Function, 14*(15), 7024–7039.

Bisht, A., Goh, K. K., Sims, I. M., Edwards, P. J., & Matia-Merino, L. (2023). Shear and temperature sensitivity of a shear-thickening biopolymer from the New Zealand black tree fern. *Food Hydrocolloids, 145*, Article 109075.

Blumenkrantz, N., & Asboe-Hansen, G. (1973). New method for quantitative determination of uronic acids. *Analytical Biochemistry, 54*(2), 484–489.

Bourbon, A. I., Pinheiro, A. C., Ribeiro, C., Miranda, C., Maia, J. M., Teixeira, J. A., & Vicente, A. A. (2010). Characterization of galactomannans extracted from seeds of *Gleditsia triacanthos* and *Sophora japonica* through shear and extensional rheology: Comparison with guar gum and locust bean gum. *Food Hydrocolloids, 24*(2–3), 184–192.

Burckbuchler, V., Kjøniksen, A.-L., Galant, C., Lund, R., Amiel, C., Knudsen, K. D., & Nyström, B. (2006). Rheological and structural characterization of the interactions between cyclodextrin compounds and hydrophobically modified alginate. *Biomacromolecules, 7*(6), 1871–1878.

Chen, H., Liu, W., Hong, M., Zhang, E., Dai, X., Chen, Q., … Ji, X. (2019). Associative behavior of polyimide/cyclohexanone solutions. *RSC Advances, 9*(47), 27455–27463.

Choi, H., Mitchell, J. R., Gaddipati, S. R., Hill, S. E., & Wolf, B. (2014). Shear rheology and filament stretching behaviour of xanthan gum and carboxymethyl cellulose solution in presence of saliva. *Food Hydrocolloids, 40*, 71–75.

Clasen, C., Plog, J., Kulicke, W.-M., Owens, M., Macosko, C., Scriven, L., … McKinley, G. H. (2006). How dilute are dilute solutions in extensional flows? *Journal of Rheology, 50*(6), 849–881.

De Ruiter, G. A., Schols, H. A., Voragen, A. G., & Rombouts, F. M. (1992). Carbohydrate analysis of water-soluble uronic acid-containing polysaccharides with high-performance anion-exchange chromatography using methanolysis combined with TFA hydrolysis is superior to four other methods. *Analytical Biochemistry, 207*(1), 176–185.

Duxenneuner, M. R., Fischer, P., Windhab, E. J., & Cooper-White, J. J. (2008). Extensional properties of hydroxypropyl ether guar gum solutions. *Biomacromolecules, 9*(11), 2989–2996.

Entov, V., & Hinch, E. (1997). Effect of a spectrum of relaxation times on the capillary thinning of a filament of elastic liquid. *Journal of Non-Newtonian Fluid Mechanics, 72*(1), 31–53.

Erni, P., Varagnat, M., Clasen, C., Crest, J., & McKinley, G. H. (2011). Microrheometry of sub-nanolitre biopolymer samples: Non-Newtonian flow phenomena of carnivorous plant mucilage. *Soft Matter, 7*(22), 10889–10898.

Franková, L., & Fry, S. C. (2013). Biochemistry and physiological roles of enzymes that 'cut and paste' plant cell-wall polysaccharides. *Journal of Experimental Botany, 64*(12), 3519–3550.

Funami, T., & Nakauma, M. (2021). Instrumental characteristics from extensional rheology and tribology of polysaccharide solutions. *Journal of Texture Studies, 52*(5–6), 567–577.

Goh, K. K. T., Matia-Merino, L., Hall, C. E., Moughan, P. J., & Singh, H. (2007). Complex rheological properties of a water-soluble extract from the fronds of the black tree fern, *Cyathea medullaris*. *Biomacromolecules, 8*(11), 3414–3421.

Goh, K. K. T., Matia-Merino, L., Pinder, D. N., Saavedra, C., & Singh, H. (2011). Molecular characteristics of a novel water-soluble polysaccharide from the New Zealand black tree fern (*Cyathea medullaris*). *Food Hydrocolloids, 25*(3), 286–292.

Hallmark, B., Bryan, M., Bosson, E., Butler, S., Hoier, T., Magens, O., … Wibberley, S. (2016). A portable and affordable extensional rheometer for field testing. *Measurement Science and Technology, 27*(12), Article 125302.

Haward, S. J., Sharma, V., Butts, C. P., McKinley, G. H., & Rahatekar, S. S. (2012). Shear and extensional rheology of cellulose/ionic liquid solutions. *Biomacromolecules, 13*(5), 1688–1699.

Holzwarth, G. (1978). Molecular weight of xanthan polysaccharide. *Carbohydrate Research, 66*(1), 173–186.

Hu, Y., Wang, S., & Jamieson, A. (1995). Rheological and rheooptical studies of shear-thickening polyacrylamide solutions. *Macromolecules, 28*(6), 1847–1853.

Iida, Y., Tuziuti, T., Yasui, K., Towata, A., & Kozuka, T. (2008). Control of viscosity in starch and polysaccharide solutions with ultrasound after gelatinization. *Innovative Food Science & Emerging Technologies, 9*(2), 140–146.

Jaishankar, A., Wee, M. S. M., Matia-Merino, L., Goh, K. K. T., & McKinley, G. H. (2015). Probing hydrogen bond interactions in a shear thickening polysaccharide using nonlinear shear and extensional rheology. *Carbohydrate Polymers, 123*, 136–145.

Jimenez, L. N., Dinic, J., Parsi, N., & Sharma, V. (2018). Extensional relaxation time, pinch-off dynamics, and printability of semidilute polyelectrolyte solutions. *Macromolecules, 51*(14), 5191–5208.

Kasehagen, L. J., & Macosko, C. W. (1998). Nonlinear shear and extensional rheology of long-chain randomly branched polybutadiene. *Journal of Rheology, 42*(6), 1303–1327.

Kjøniksen, A.-L., Hiorth, M., & Nyström, B. (2005). Association under shear flow in aqueous solutions of pectin. *European Polymer Journal, 41*(4), 761–770.

Kongjaroen, A., Methacanon, P., & Gamonpilas, C. (2022). On the assessment of shear and extensional rheology of thickened liquids from commercial gum-based thickeners used in dysphagia management. *Journal of Food Engineering, 316*, Article 110820.

Lai, L.-S., & Liang, H.-Y. (2012). Chemical compositions and some physical properties of the water and alkali-extracted mucilage from the young fronds of *Asplenium australasicum* (J. Sm.) Hook. *Food Hydrocolloids, 26*(2), 344–349.

Liu, G., Sun, H., Rangou, S., Ntetsikas, K., Avgeropoulos, A., & Wang, S.-Q. (2013). Studying the origin of "strain hardening": Basic difference between extension and shear. *Journal of Rheology, 57*(1), 89–104.

Ma, S. X., & Cooper, S. L. (2001). Shear thickening in aqueous solutions of hydrocarbon end-capped poly (ethylene oxide). *Macromolecules, 34*(10), 3294–3301.

McCleary, B., & Matheson, N. (1974). α-D-Galactosidase activity and galactomannan and galactosylsucrose oligosaccharide depletion in germinating legume seeds. *Phytochemistry, 13*(9), 1747–1757.

McKinley, G. H., & Tripathi, A. (2000). How to extract the Newtonian viscosity from capillary breakup measurements in a filament rheometer. *Journal of Rheology, 44*(3), 653–670.

Nep, E. I., Carnachan, S., Ngwuluka, N., Kontogiorgos, V., Morris, G., Sims, I., & Smith, A. M. (2016). Structural characterisation and rheological properties of a polysaccharide from sesame leaves (*Sesamum radiatum* Schumach. & Thonn.). *Carbohydrate Polymers, 152*, 541–547.

Piermaría, J., Bengoechea, C., Abraham, A. G., & Guerrero, A. (2016). Shear and extensional properties of kefiran. *Carbohydrate Polymers, 152*, 97–104.

Reid, J. S. G., & Meier, H. (1973). Enzymic activities and galactomannan mobilisation in germinating seeds of fenugreek (*Trigonella foenum-graecum* L. Leguminosae). *Planta, 112*(4), 301–308.

Rodd, L. E., Scott, T. P., Cooper-White, J. J., & McKinley, G. H. (2005). Capillary break-up rheometry of low-viscosity elastic fluids. *Applied Rheology, 15*(1), 12–27.

Sims, I. M., & Newman, R. H. (2006). Structural studies of acidic xylans exuded from leaves of the monocotyledonous plants *Phormium tenax* and *Phormium cookianum*. *Carbohydrate Polymers, 63*(3), 379–384.

Szopinski, D., Handge, U. A., Kulicke, W.-M., Abetz, V., & Luinstra, G. A. (2016). Extensional flow behavior of aqueous guar gum derivative solutions by capillary breakup elongational rheometry (CaBER). *Carbohydrate Polymers, 136*, 834–840.

Tam, K. C., Jenkins, R. D., Winnik, M. A., & Bassett, D. R. (1998). A structural model of hydrophobically modified urethane–ethoxylate (HEUR) associative polymers in shear flows. *Macromolecules, 31*(13), 4149–4159.

Tan, H., Tam, K. C., & Jenkins, R. D. (2001). Network structure of a model HASE polymer in semidilute salt solutions. *Journal of Applied Polymer Science, 79*(8), 1486–1496.

Tirtaatmadja, V., McKinley, G. H., & Cooper-White, J. J. (2006). Drop formation and breakup of low viscosity elastic fluids: Effects of molecular weight and concentration. *Physics of Fluids, 18*(4), Article 043101.

Torres, M. D., Hallmark, B., & Wilson, D. I. (2014). Effect of concentration on shear and extensional rheology of guar gum solutions. *Food Hydrocolloids, 40*, 85–95.

Vadillo, D. C., Mathues, W., & Clasen, C. (2012). Microsecond relaxation processes in shear and extensional flows of weakly elastic polymer solutions. *Rheologica Acta, 51*(8), 755–769.

Vasilyev, G. B., Dreval, V. E., Malkin, A. Y., & Kulichikhin, V. G. (2010). Rheology of linear and branched styrene–acrylonitrile copolymers. Similarities and differences. *Polymer Science, Series A, 52*(11), 1142–1155.

Wagner, M. H., Bastian, H., Hachmann, P., Meissner, J., Kurzbeck, S., Münstedt, H., & Langouche, F. (2000). The strain-hardening behaviour of linear and long-chain-branched polyolefin melts in extensional flows. *Rheologica Acta, 39*(2), 97–109.

Wagner, R., Simas, F. F., Pereira, G. C. Z., Angeli, A., Brito, J. O., Woranovicz-Barreira, S. M., … Gorin, P. A. J. (2007). Structure of a glycoglucuronomannan from the gum exudate of *Vochysia tucanorum* (family Vochysiaceae). *Carbohydrate Polymers, 69*(3), 512–521.

Wagner, R., Simas, F. F., Sassaki, G. L., Iacomini, M., da Silva, M. A., & Gorin, P. A. J. (2008). A high-viscosity glycoglucuronomannan from the gum exudate of *Vochysia thyrsoidea*: Comparison with those of other Vochysia spp. *Carbohydrate Polymers, 72*(3), 382–389.

Wagner, R., Woranovicz-Barreira, S. M., Iacomini, M., Delgobo, C. L., Pimentel, N. M., & Gorin, P. A. J. (2004). Structure of a glycoglucuronomannan from the low-viscosity gum of *Vochysia lehmannii*. *Carbohydrate Polymers, 57*(3), 269–275.

Wang, D., Yeats, T. H., Uluisik, S., Rose, J. K., & Seymour, G. B. (2018). Fruit softening: Revisiting the role of pectin. *Trends in Plant Science, 23*(4), 302–310.

Ward, O. P., Moo-Young, M., & Venkat, K. (1989). Enzymatic degradation of cell wall and related plant polysaccharides. *Critical Reviews in Biotechnology, 8*(4), 237–274.

Wee, M. S. M., Matia-Merino, L., Carnachan, S. M., Sims, I. M., & Goh, K. K. T. (2014). Structure of a shear-thickening polysaccharide extracted from the New Zealand black tree fern, *Cyathea medullaris*. *International Journal of Biological Macromolecules, 70*, 86–91.

Wee, M. S. M., Matia-Merino, L., & Goh, K. K. T. (2015). The cation-controlled and hydrogen bond-mediated shear-thickening behaviour of a tree-fern isolated polysaccharide. *Carbohydrate Polymers, 130*, 57–68.

Wunderlich, T., Stelter, M., Tripathy, T., Nayak, B., Brenn, G., Yarin, A., … Durst, F. (2000). Shear and extensional rheological investigations in solutions of grafted and ungrafted polysaccharides. *Journal of Applied Polymer Science, 77*(14), 3200–3209.

Xu, D., Hawk, J. L., Loveless, D. M., Jeon, S. L., & Craig, S. L. (2010). Mechanism of shear thickening in reversibly cross-linked supramolecular polymer networks. *Macromolecules, 43*(7), 3556–3565.

Yesilata, B., Clasen, C., & McKinley, G. H. (2006). Nonlinear shear and extensional flow dynamics of wormlike surfactant solutions. *Journal of Non-Newtonian Fluid Mechanics, 133*(2–3), 73–90.

Yuan, B., Ritzoulis, C., & Chen, J. (2018). Extensional and shear rheology of a food hydrocolloid. *Food Hydrocolloids, 74*, 296–306.